In-situ synthesis of a plasmonic Ag/AgCl/Ag$_2$O heterostructures for degradation of ciprofloxacin

Songbo Yang [a], Dongbo Xu [a,b], Biyi Chen [a], Bifu Luo [a], Weidong Shi [a,*]

[a] School of Chemistry and Chemical Engineering, Jiangsu University, Zhenjiang 212013, PR China
[b] School of Energy and Power Engineering, Jiangsu University, Zhenjiang 212013, PR China

ABSTRACT

Ciprofloxacin (CIP) has caused serious environmental problems because of its high resistance to conventional wastewater treatments methods. To improve the photodegradation efficiency for CIP, a new system of Ag/AgCl/Ag2O is developed by growth of Ag/AgCl on the surface of Ag2O nonoparticles at room temperature. The stable Ag/AgCl nanoshells could efficiently protect inner Ag2O from photocorrosion during the photocatalytic process and enhance the separation and transfer efficiency of photo-induced electron–hole pairs. The optimum photocatalytic efficiency of 50% Ag/AgCl/Ag2O heterostructures for the degradation of CIP under visible light irradiation ($\lambda > 420$ nm) was about 2.9 and 3.73 times higher than that of individual Ag2O and Ag/AgCl, respectively. The radical trap experiments showed that the degradation of CIP was driven mainly by the participation of superoxide radical (O2$^{-\bullet}$) and the action of holes (h$^+$). From the experimental results and the relative band gap position of these semiconductors, a possible Z-scheme photocatalytic mechanism was proposed. The system has greatly overcome the drawbacks of single component Ag2O and realized the strong redox ability and long-term stability.

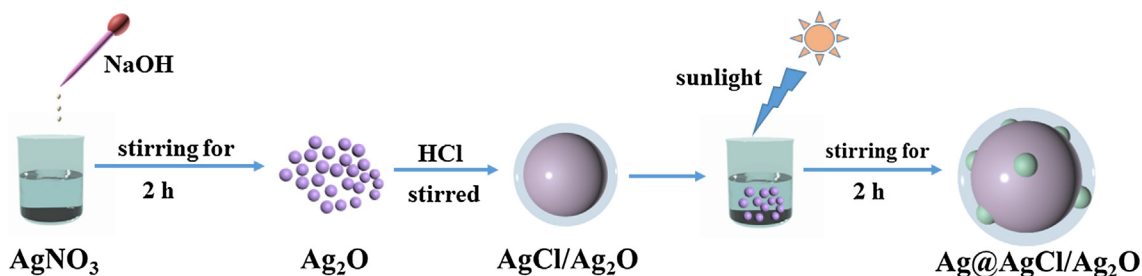© 2016 Elsevier B.V. All rights reserved.

1. Introduction

Ciprofloxacin (CIP), as a third generation of fluoroquinolones (FQs) antibiotic, is widely used for treating bacterial infection because of its broad-spectrum antibacterial activity [1–4]. This antibacterial agent is largely used both in human and veterinary medicine, but it is only partially metabolized in the body. human pharmaceuticals or their metabolites would be introduced into the aquatic environment, which may cause serious threats to the ecosystem and human health due to the possible development of resistance in pathogens [5,6]. The elimination of CIP from the environment has already become an urgent issue, which attracts the wide attention of researchers [7,8]. Owing to its resistance to microbiological degradation, the conventional physical and chemical treatments are not able to eliminate CIP residues efficiently. Compared to traditional treatments, the photocatalytic oxidation has provided to be a good tool for the transformation and degradation of CIP [9]. Some researchs about the efficient photocatalytic degradation of CIP by semiconductor-based (such as TiO$_2$ and ZnO) photocatalysts have been reported [10,11]. But these traditional photocatalysts often operate with ultraviolet light, which accounts

for only 4% of the incoming solar energy. As a result, the development of a visible-light-driven photocatalysts with further enhanced conversion efficiency is indispensable for the practical use of solar energy.

Silver (I) oxide (Ag$_2$O) is a p-type semiconductor with a reported band gap of 1.2 eV [12]. It has been recognized as one of the most promising alternatives to the traditional photocatalysts because of its excellent absorption capacity of visible light and extremely high photo-oxidative capabilities for organic contaminant [13–15]. However, Ag$_2$O greatly suffers from poor stability and rapid recombination of photogenerated electronehole pairs in practical applications. Formation of the heterostructures between two semiconductors can not only prominently increase light-harvesting efficiency but also promote charge separation and transfer effectively. Yu et al. [16] synthesized the Ag$_2$O/Ag$_2$CO$_3$ heterostructures via phase transformation route, which exhibits extremely high activity and stability in photocatalytic degradation of pollutants. Yu. Bi et al. [17] reported that the AgX/Ag$_3$PO$_4$ (X = Cl, Br, I) heterostructures exhibit much higher photocatalytic activities, structural stabilities and photoelectric properties than pure Ag$_3$PO$_4$. These results indicate that fabrication of the phase interface/junctions between the photocatalytic semiconductors could be effective in improving the photocatalytic activity due to electronic interaction and electron transfer at the heterostructures interfaces. However, the synthesis of Ag$_2$O based nanocomposites

Scheme 1. Schematic illustration of the preparation Ag/AgCl/Ag$_2$O heterostructures.

with high the strong redox ability and long-term stability is still a big challenge.

Recently, Silver chloride (AgCl) as a photosensitive semiconductor material with a bandgap of 3.25 eV, is considered to be one of the most promising photocatalysts [18–22]. Although the intrinsic light response of AgCl locates in the UV region, AgCl nanoparticles could generate electron–hole pairs when they absorb photos, and subsequently the photogenerated electrons combines with an Ag$^+$ ion to form an Ag^0 atom, which could extend the light response of AgCl into the visible light region [23–25]. Recently, numerous studies have been carried out to couple various semiconductors with Ag/AgCl to enhance their photocatalytic activities. For example, it has been reported that Ag/AgCl/BiVO$_4$ [26], Ag/AgCl/Bi$_2$WO$_6$ [27], Ag/AgCl/g-C$_3$N$_4$ [28], Ag/AgCl/TiO$_2$ [29], Ag/AgCl@WO$_3$ [30], AgCl/Ag/γ-TaON [31] and Ag/AgX/BiOX (X = Cl, Br) [32] showed enhanced visible light photocatalytic activity. However, there is still no reportes on synthesis of the Ag/AgCl/Ag$_2$O heterostructures. It is likely that an excellent redox ability can be achieved in the photocatalytic system obtained by combining Ag/AgCl with Ag$_2$O.

In the present work, a new Ag/AgCl/Ag$_2$O heterostructures were synthesized via a in-situ growth strategy for the first time. The prepared samples showed high visible-light photocatalytic activity and stability for photocatalytic degradation of Ciprofloxacin (CIP) aqueous solution. The optimum photocatalytic efficiency of 50% Ag/AgCl/Ag$_2$O heterostructures for the degradation of CIP was about 2.9 and 3.73 times higher than that of individual Ag$_2$O and Ag/AgCl, respectively. A possible mechanism toward the photocatalysis of the Ag/AgCl/Ag$_2$O heterostructures has been studied, and a plasmonic Z-scheme mechanism was proposed based on the active species trapping experiments.

2. Experimental

2.1. Preparation of Ag$_2$O nanoparticles

Pure Ag$_2$O were prepared by a simple precipitation method at room temperature. In a typical synthesis program, 0.153 g AgNO$_3$ was dispersed in 25 mL deionized water, vigorously stirred for 2 h. Then, 25 mL of 0.05 M NaOH was added drop into the suspension, and then followed by a washing and Collection process.

2.2. Preparation of Ag/AgCl/Ag$_2$O heterostructures

Ag/AgCl/Ag$_2$O heterostructures were prepared by the obtained Ag$_2$O nanoparticles further reacting with appropriate hydrochloric acid (0.1 M). In such a process, Ag$_2$O nanoparticles were used as both template and silver ion source. The surface of Ag$_2$O nanoparticles could be readily reacted with chloride ion to form AgCl nanoparticles. Finally, the as-prepared AgCl/Ag$_2$O were dispersed in water under stirring and then irradiated with sunlight for 2 h to produce Ag/AgCl/Ag$_2$O heterostructure. According to this method, different molar ratio of Ag/AgCl/Ag$_2$O samples were obtained, and the samples were denoted as x - Ag/AgCl/Ag$_2$O (x means the molar

percentage of Ag/AgCl). The process is shown in Scheme 1. The reference Ag/AgCl was obtained by the simple precipitation reaction of AgNO$_3$ and hydrochloric acid solution.

2.3. Characterization

The phase and composition of the as-prepared samples were detected by X-ray diffraction (XRD) studies using an X-ray diffractometer with Cu Kα radiation under 40 kV and 40 m A with ranging from 10° to 80° at a scanning rate of 4.0° min^{-1} (Bruker AXS, Germany). The morphologies and microstructures of the as-prepared samples were obtained by resolution transmission electron microscopy (TEM, FEI JEM-2100 and FEI Tecnai G2 F20), and high-resolution TEM (HRTEM) images were examined by transmission electronmicroscopy (Tenai G2 F30 S-Twin, FEI) with an accelerating voltage of 200 kV. The scanning electron microscopy (SEM) images were obtained on a Hitachi S-4800 II, Japan. The X-ray photoelectron spectroscopy was performed with a VG ESCALAB 250 spectrometer using a nonmonochromatized Al Kα X-ray source. The UV–vis diffuse reflectance spectra (DRS) of the samples were recorded with a UV–vis spectrophotometer (Shimadzu UV-3100) using BaSO$_4$ was used as a reflectance standard.

2.4. Photoelectrochemical measurements

The transient photocurrent responses and electrochemical impedance spectra (EIS) of the samples were determined using a CHI660D electrochemical working station in a three-electrode quartz cell with Na2SO4 (0.1 M) electrolyte solution. A Pt wire as the counter electrode, and Ag/AgCl (satu-rated KCl) as a reference electrode. A 50 W Xe arc lamp served as a light source.

2.5. Photocatalytic activity

The photocatalytic activities of the prepared samples were evaluated by degradation of CIP aqueous solution under visible light irradiation. The photochemical reactor was illuminated using a 250 W xenon lamp with a 420 nm cutoff filter. Experimental details were shown as follows: 0.1 g of the sample was dispersed into 100 mL of 10 mg/L pollutants aqueous solution. The solution was stirred in the dark for 30 min to reach an adsorption–desorption equilibrium among the photocatalyst, CIP, and water before visible-light irradiation. During photocatalytic processes, 5 mL of the suspension was taken out and centrifuged (10,000 rpm, 6 min) to separate the photocatalyst powder from the solution, and used for the absorbance measurement by a TU-1810 UV–vis spectrophotometer. The peak absorbencies of CIP at 277 nm were used to determine its concentration.
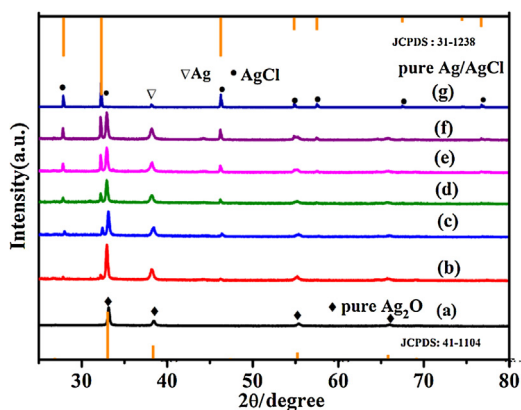
Fig. 1. XRD patterns for the as-prepared samples: (a) Ag$_2$O, (b) 10% Ag/AgCl/Ag$_2$O, (c) 30% Ag/AgCl/Ag$_2$O, (d) 50% Ag/AgCl/Ag$_2$O, (e) 70% Ag/AgCl/Ag$_2$O, (f) 90% Ag/AgCl/Ag$_2$O, and (g) Ag/AgCl.

3. Results and discussion

3.1. Structural characterization

The crystal structures of the serial samples were studied by XRD and the result is shown in Fig. 1, in pure Ag/AgCl samples, the diffraction peaks at 2θ = 27.9° (d = 0.319 nm), 32.4° (d = 0.276 nm), 46.4° (d = 0.195 nm), 55.1° (d = 0.166 nm), 57.6° (d = 0.159 nm), 67.5° (d = 0.138 nm), 74.5° (d = 0.127 nm) and 76.9° (d = 0.124 nm) correspond to the (111), (200), (220), (311),(222), (400), (331) and (420) planes of the cubic phase of Ag/AgCl with lattice constant a = 0.555 nm (JCPDS file: 31–1238) [29]. The diffraction peaks at 2θ = 32.8°, 38.1°, 54.9°, and 65.4° correspond to the well-crystallized cubic Ag$_2$O (JCPDS 41-1104) [33,34]. a weak diffraction peak at 2θ = 38.1° can be ascribed to the (111) plane of the cubic phase of Ag (JCPDS card 04-0783) [26], indicting that the Ag nanoparticles (NPs) are formed. No any other impurities were detected, showing that the products are pure phase. Furthermore, we can see that the peaks of AgCl gradually increase with concentration of Cl$^-$ increasing, indicating we successfully prepared the Ag/AgCl/Ag$_2$O nanocomposites with different molar ratios.

After the Ag$_2$O reacted with the HCl, the AgCl NPs grew in situ on the Ag$_2$O surface. To investigate the morphology of the Ag/AgCl/Ag$_2$O, SEM imaging was performed, and the results are presented in Fig. 2. As shown in Fig. 2a, Ag$_2$O displays the particle structure and its size is about 100–200 nm. Fig. 1(b–c) shows the FESEM images of Ag/AgCl/Ag$_2$O heterostructures. These nanoparticles exhibit cube-like morphologies and uniform sizes with average 200 nm. When AgCl NPs grew in situ on the Ag$_2$O surface, both the sizes and morphologies have significantly changed, indicating the synthesis of the Ag/AgCl/Ag$_2$O heterostructure. The energy dispersive X-ray spectroscopy (EDS) analysis is employed to further identify the elements component of the heterostructure, and the
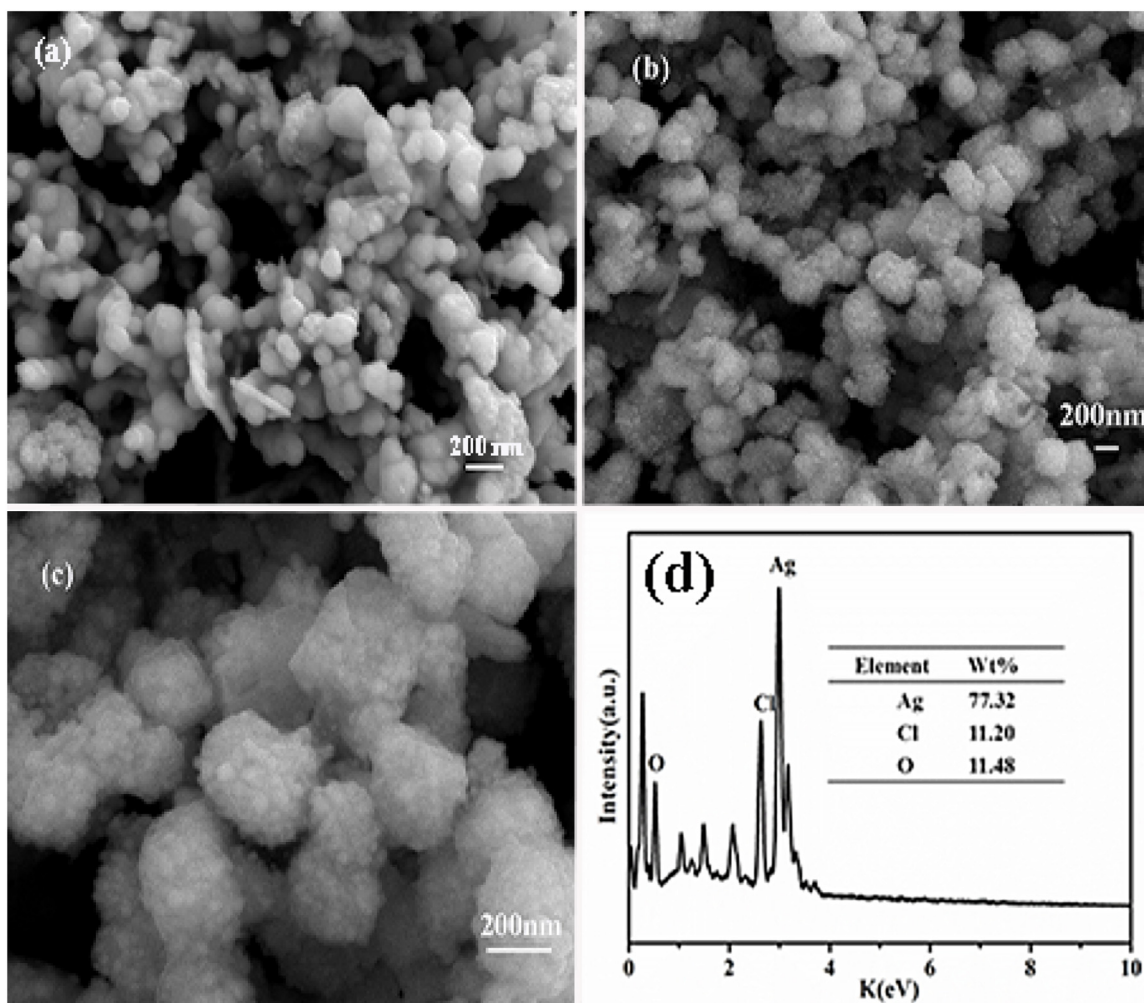

Fig. 2. SEM images of the as-prepared samples: (a) pure Ag$_2$O (b–c) 50% Ag/AgCl/Ag$_2$O heterostructures. (d)EDS spectrum of 50% Ag/AgCl/Ag$_2$O heterostructures.

Fig. 3. TEM images of (a) Ag$_2$O nanoparticles, (b)–(c) 50% Ag/AgCl/Ag$_2$O heterostructures (d) HRTEM image of 50% Ag/AgCl/Ag$_2$O heterostructures.

corresponding EDS spectrum is shown in Fig. 2d. It can be seen that the elements in the composite are Ag, Cl, and O, which were indicative of the Ag, AgCl, and Ag$_2$O components present in the heterostructure. According to the calculation, the atomic ratio of Cl to O was found to be about 1:2, which is correspond to the theoretical molar ratio of the 50% Ag/AgCl/Ag$_2$O samples.

To further obtain the morphology and structure information, the TEM and HRTEM analysis of the pure Ag$_2$O and Ag/AgCl/Ag$_2$O heterostructures have been applied (Fig. 3). As shown in Fig. 3a, the pure Ag$_2$O nannoparticles were found to range from approximately 100 to 200 nm. The sample containing Ag/AgCl deposited onto Ag$_2$O prepared by self-assembly method is shown in Fig. 3b–c, after the Ag$_2$O reacted with the HCl, the AgCl components grew in situ on the Ag$_2$O surface. The thin Ag/AgCl layer with a thickness of 5–10 nm was observed in Ag/AgCl/Ag$_2$O heterostructures in Fig. 3c. As shown in Fig. 3b, some spherical particles with an average diameter of approximately 20 nm were observed to be uniformly anchored on the surface of Ag$_2$O, which were thought to be the Ag/AgCl nanoparticles forming in the stirring process. The results consistent with SEM results. The HR-TEM image (Fig. 3d) of the sample indicated the lattice spacing of Ag, AgCl and Ag$_2$O, the

resolved interplanar distance of 0.27 nm agrees well with the lattice spacing of the (111) plane of Ag$_2$O, and 0.24 and 0.28 nm, are in good agreement with the crystal planes for the (111) and (200) faces of Ag and AgCl, respectively. [12,27] The above results further indicate the as formed Ag/AgCl samples were closely combined to the surface of the Ag$_2$O nanoparticles for the formation of the heterostructures interface, which could be profitable for the electron transfer between the Ag/AgCl and Ag$_2$O, resulting in an enhanced electron–hole separation efficiency.

The XPS was carried out to investigate the chemical composition and the valence states of the prepared samples. The narrow-scan XPS spectra of the C 1s, O 1s, Cl 2p and Ag 3d peaks for the surface of the Ag/AgCl/Ag$_2$O heterostructures are shown in Fig. 4a. The peak of which C1s is due to the adventitious hydrocarbon from the XPS instrument itself. The survey XPS spectrum (Fig. 4a) of the prepared samples confirmed the main ingredient elements of Ag, O and Cl, which agreed well with the results of EDS analysis (Fig. 2d). The high-resolution XPS spectra in Fig. 4b–d shows the characteristic peaks of Ag 3d, Cl 2p and O 1s of Ag/AgCl/Ag$_2$O heterostructures. The Ag 3d region in Fig. 4b gives two obvious peaks at 368.21 and 374.2 eV, which are ascribed to Ag 3d5/2 and Ag 3d3/2, respec-
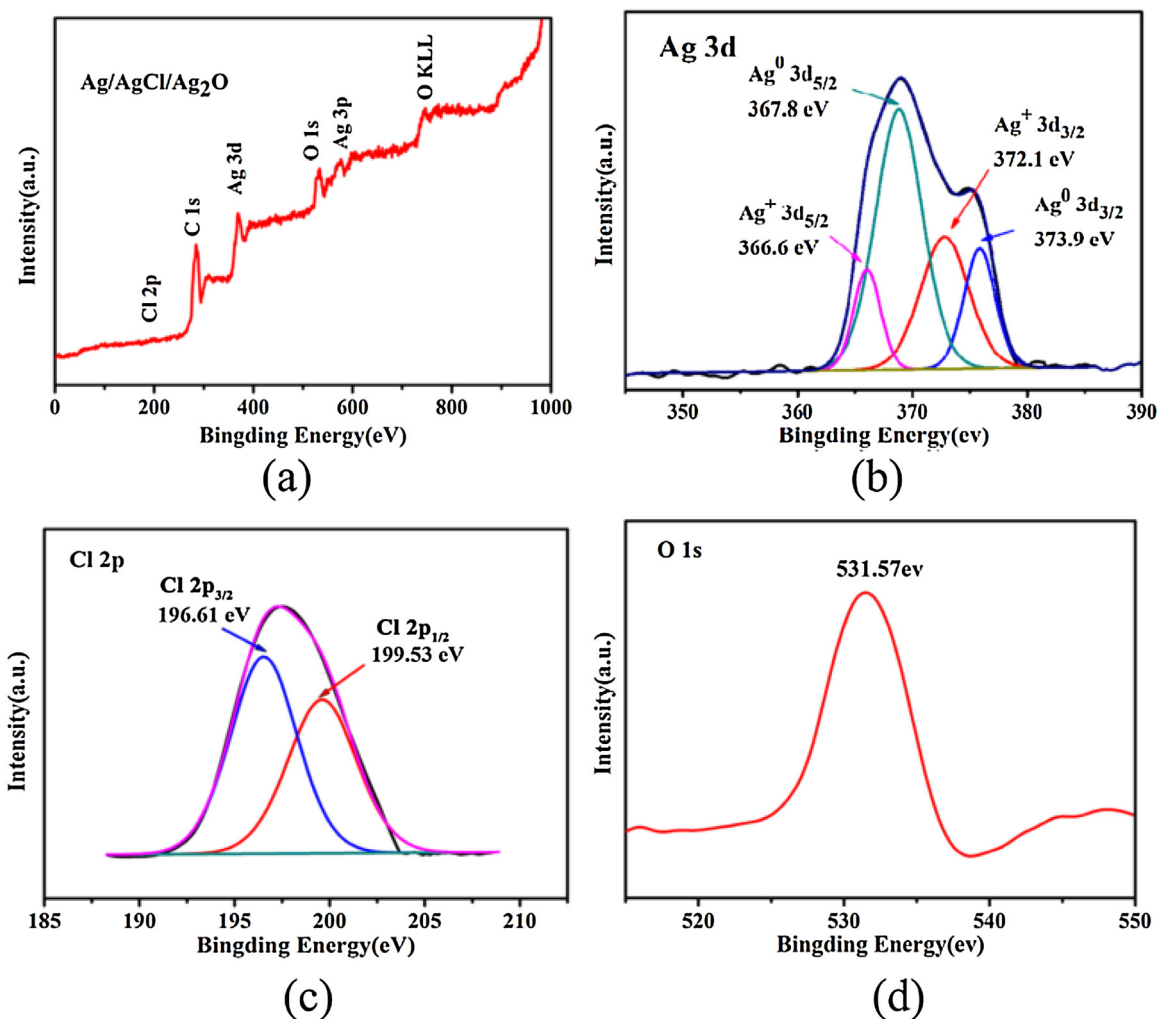
Fig. 4. XPS spectra of the Ag/AgCl/Ag$_2$O heterostructures. (a) The survey XPS spectrum, (b) Ag 3d, (c) Cl 4f, (d) O 1s peaks related to the photocatalyst.

tively. These two bands can be further divided into different peaks at 366.6, 367. 8 as well as 373.1 and 374.9 eV. The bands at 366.6 and 373.1 eV are attributed to the Ag$^+$ of AgCl and Ag$_2$O, and those at 367.8 and 374.9 eV are ascribed to the metallic Ag^0. These results further corroborated the existence of metallic Ag^0 in Ag/AgCl/Ag$_2$O heterostructures. Similar results are reported by other researchers. [35,36] The deconvoluted peaks for the Cl 2p orbits were centred at approximately 199.53 and 196.61 eV, respectively, which are ascribedto the binding energies of Cl 2p 1/2 and Cl 2p 3/2 deriving from Cl$^-$ (Fig. 4c, AgCl).[21] Fig. 4d shows the XPS spectra of O 1s, where peaks at 531.57 eV, corresponding to O^{2-} from Ag$_2$O.

The UV−vis spectra of pure Ag$_2$O, Ag/AgCl, and different ratios of Ag/AgCl/Ag$_2$O photocatalysts are shown in Fig. 5, Ag$_2$O exhibited a wide and strong light absorption in the whole UV−vis range of 200–700 nm, which confirmed its excellent light absorption activity. As for the Ag/AgCl photocatalysts exhibited broad absorption, owing to the surface plasmon resonance (SPR) of Ag NPs, coming from the photochemical decomposition of AgCl [37]. When the 50% Ag/AgCl coated with Ag$_2$O, the visible-light responses of the composites were slightly improved, meaning that the LSPR effect and the formation of heterostructures contributed prominently to the enhanced photocatalytic activity. Furthermore, the results of UV−vis DRS showed that the Ag/AgCl/Ag$_2$O heterostructures could improve the absorption property and increase the utilization efficiency of solar light.
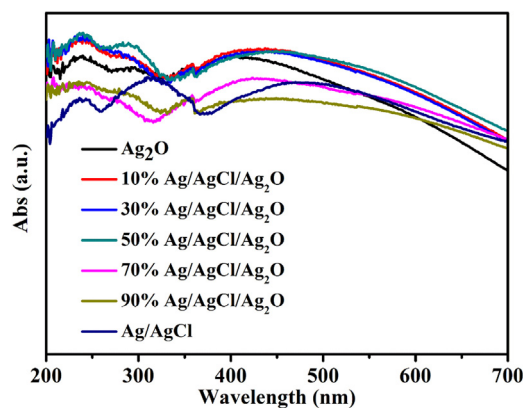

Fig. 5. UV–vis spectra of the pure Ag$_2$O, Ag/AgCl and Ag/AgCl/Ag$_2$O heterostructures with 10%, 30%, 50%, 70% and 90% Ag/AgCl loaded.

It is well acknowledged that stronger photocurrent intensity suggests higher photoinduced charge carrier's separation and migration efficiency. As is shown in Fig. 6a, the photocurrent for Ag/AgCl/Ag$_2$O heterostructures were much higher than that of pure Ag/AgCl and pure Ag$_2$O when light was on, which indicated that the mobility and separation efficiency of the photo-induced carriers was efficaciously improved after Ag/AgCl loading on the surface
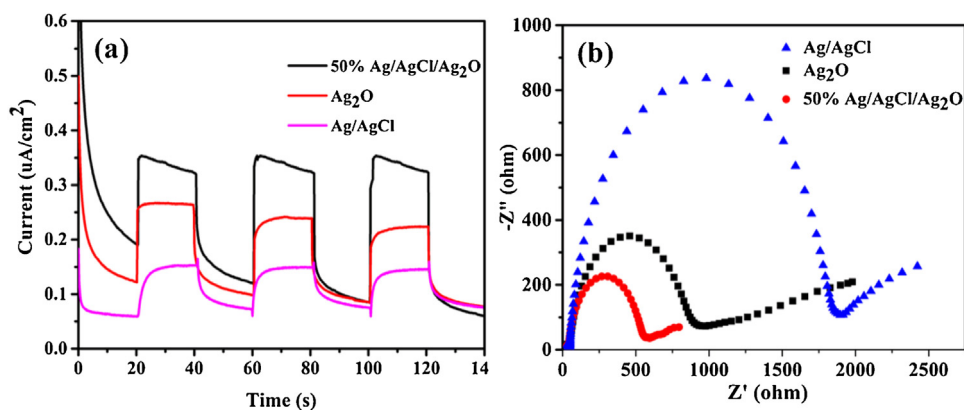
Fig. 6. (a) electrochemical impedance and (b) photocurrent responses spectra of as-prepared samples.

of Ag_2O. In addition, EIS measurement was also carried out to investigate the charge transfer resistance and the separation efficiency of the photoinduced charge carrier. The radius of the arc on the EIS Nyquist plot represented the charge transfer step occurring at the surface of the electrode. [38] As can be seen from Fig. 6b, the diameter of the Nyquist semicircle for the heterostructures were lower than that of Ag/AgCl and Ag_2O, indicating the heterostructure have a lower resistance. The result of EIS plot demonstrated that the separation efficiency of photogenerated electronic-hole pairs increased in the order of Ag/AgCl, Ag_2O and Ag/AgCl/Ag_2O heterostructures, which was in good agreement with the photocurrent measurements. This result demonstrates that the interface of the Ag/AgCl and Ag_2O can enhance the separation and transfer efficiency of photoinduced electron–hole pairs.

3.2. Photocatalytic activity and stability

The photocatalytic activity of the as-prepared Ag/AgCl/Ag_2O heterostructures were investigated for photodegradation of Ciprofloxacin (CIP) under visible light irradiation ($\lambda > 420$ nm). As shown in Fig. 7a, the pure Ag_2O samples exhibit low photocatalytic performance for degradation of CIP under visible light. After combining Ag/AgCl and Ag_2O, the photocatalytic activity of the heterostructures is significantly improved for the degradation of CIP compared with the individual Ag_2O and Ag/AgCl. Among them, the highest activity is obtained over the 50% Ag/AgCl/Ag_2O heterostructures, resulting in a 91.2% degradation ratio of CIP within 100 min under visible light irradiation. The optimum photocatalytic efficiency of 50% Ag/AgCl/Ag_2O samples for the degradation of CIP was about 2.9 and 3.73 times higher than that of individual Ag_2O and Ag/AgCl, respectively. The result indicted the loading of Ag/AgCl in composites had a crucial influence on photocatalytic activity. When the Ag/AgCl content is increased beyond 50%, a decrease in the photocatalytic activity was observed. It may be attributed to the excess Ag/AgCl may decrease the quality of effective heterointerfaces in the Ag/AgCl/Ag_2O heterostructures and weaken the absorption of visible light absorption. To quantitatively compare the photocatalytic activities of these samples, the kinetic behavior of photocatalytic degradation using these Ag/AgCl/Ag_2O heterostructures were investigated further. As illustrated in Fig. 7b, the corresponding plot of $-\ln(C/C_0) \sim t$ exhibits a good linearity, further confirming the first-order kinetic model:

$$\ln C_0/C = kt$$

Where C is the concentration of CIP remaining in the solution at irradiation time of t, C_0 is the initial concentration at t = 0, and k is the degradation apparent rate constant. Fig. 7c presents the UV–vis spectra changes of CIP aqueous solution over 50% Ag/AgCl/Ag_2O

heterostructures under visible light irradiation. The maximum absorption of the CIP suspension shifts from 277 to 260 nm due to cycloreversion and the removal of group, [3,39] and the absorption intensity rapidly decreases with the increase of irradiation time. The results further demonstrate that the CIP molecules are nearly degraded in a stepwise manner after 100 min under visible light irradiation. The activity stability was checked by repeating the photocatalytic degradation processes four times, as shown in Fig. 7d. we found that the photocatalytic activity of the Ag/AgCl/Ag_2O heterostructures do not have noticeable change after four recycles for the degradation of CIP, and the slight decrease should originated from the inescapable loss of catalyst during the recycling process. The results indicated that the Ag/AgCl/Ag_2O heterostructures had high and stable activity for photocatalytic decomposition of CIP in solutions.

The mineralization efficiency was calculated from total organic-carbon (TOC) measurements. As shown in Fig. 8, The TOC removal rates of CIP in 100 min reached 55.6%, which is lower than that of the DR (91.2%). This indicated that CIP degradation occurred in multiple steps and some steps generate only intermediates rather than CO2. The results also consistent with the UV–vis spectral absorption changes of CIP solution.

3.3. Proposed photocatalytic mechanism

In order to further reveal the photocatalytic mechanism of Ag/AgCl/Ag_2O heterostructures, we also used the different active species trapping experiments for the degradation of CIP over the pure Ag_2O, AgCl and 50% Ag/AgCl/Ag_2O samples to explore the enhancing photocatalytic mechanism. As shown in Fig. 9a, for pure Ag_2O, when 1 mmol isopropyl alcohol (IPA) as scavenger for $^\bullet$OH radical species was added into reaction solution, the photocatalytic degradation rate is almost invariable. When 1 mmol of $O_2^{-\bullet}$ scavenger vitamin C (VC) was added into reaction solution, the photocatalytic degradation rate is slightly inhibited. However, when the TEA was added into reaction solution, the degradation rate of CIP reduced significantly. Thus, the holes (h^+) are the major reactive species in the pure Ag2O reaction system. On the contrary, for AgCl, when the VC and TEA ware added into reaction solution, the photocatalytic degradation rate is almost inhibited. When the IPA was added, the degradation rate of CIP almost no changed, implying that the h^+ and $O_2^{-\bullet}$ were the major reactive species in the pure AgCl reaction system. On the other hand, for the 50% Ag/AgCl/Ag_2O sample, the photocatalytic activity is similar to the blank by the addition of IPA, indicating that $^\bullet$OH was not reactive species involved in the degradation of CIP process. However, the degradation of CIP was remarkably prohibited with the addition of VC, suggesting that the $O_2^{-\bullet}$ pathways play a crucial role in the process of CIP oxidation.
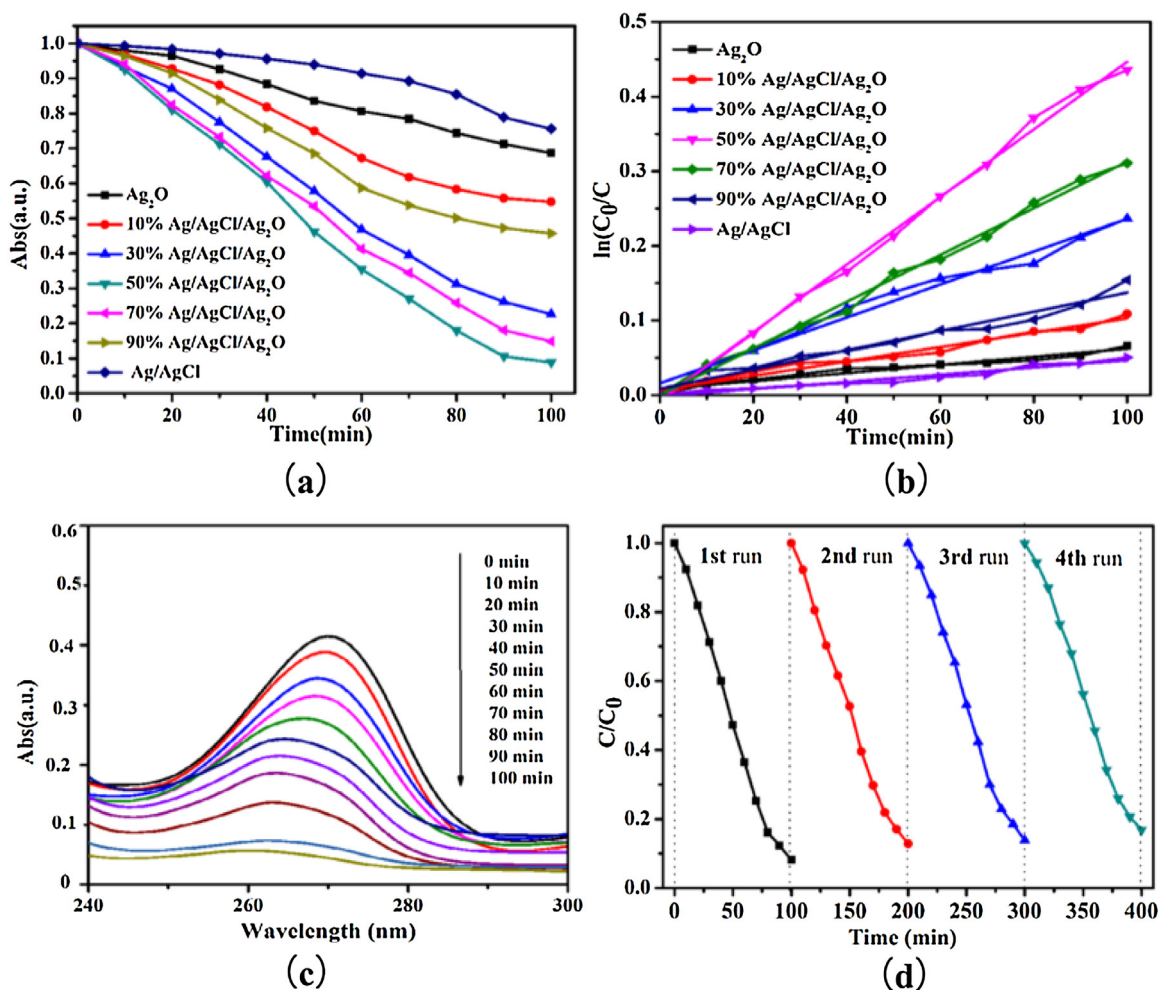
Fig. 7. (a) Photodegradation of CIP in the presence of different samples under visible-light irradiation. (b) Photodegradation kinetics of CIP aqueous solutions over various photocatalysts. (c). The UV–vis spectral absorption changes of CIP solution photodegraded over 50% Ag/AgCl/Ag₂O heterostructures. (d) Cycling runs of the 50% Ag/AgCl/Ag₂O heterostructures degradation of CIP.

The degradation efficiency of CIP was also reduced significantly upon the introduction of (TEA), indicating that the holes (h^+) also played a large role in the photocatalytic degradation process. Based on the above results, we can conclude that the holes and $O_2^{-\bullet}$ radicals are the predominant active species, while $^\bullet OH$ almost had no influence in the photodecomposition behavior in the presence of 50% Ag/AgCl/Ag₂O heterostructures.

According to the experiment reported previously, the positions of the conduction and the valence bands of Ag₂O was determined to be o.2 eV and 1.4 eV (vs. SHE), respectively [12]. The conduction band (CB) and valence band (VB) energy levels of AgCl are ca. −0.06 eV and 3.2 eV (vs. SHE) [26]. The visible light absorptionin AgCl with wide band gap of 3.25 eV can be attributed to the plasmonic absorption of metallic Ag nanoparticles (Ag/AgCl). Considering the $O_2^{-\bullet}$ is one of the main active species, electrons in the CB of A₂O could not reduce O_2 to generate $O_2^{-\bullet}$ active species because the CB potential of Ag₂O 0.2 eV (vs. SHE) is more positive than the reduction potential of oxygen E^0 ($O_2/O_2^{-\bullet}$) −0.046 eV (vs. SHE) [30,40]. On the basic of the above experimental results, a plasmonic Z-scheme mechanism of the Ag/AgCl/Ag₂O heterostructure was proposed. As illustrated in Scheme 2, the plasmon-induced electrons of Ag nanoparticles are injected into the CB of AgCl to reduce O_2 to produce $O_2^{-\bullet}$ because of the relative negative conduction band (CB) potential of AgCl −0.09 eV (vs. SHE) to $O_2/O_2^{-\bullet}$ −0.046 eV (vs. SHE) [41], while the holes remain on the Ag nanopar-
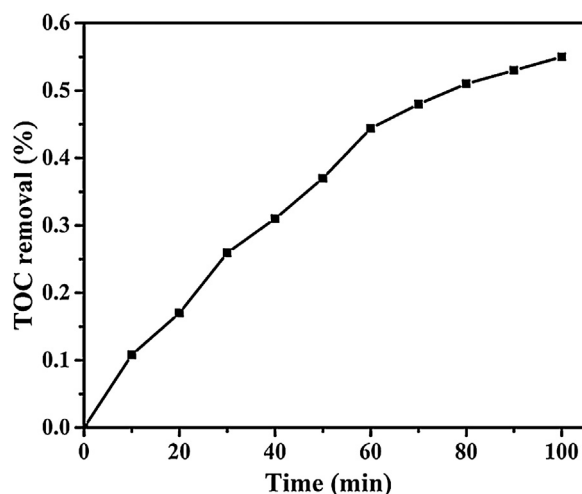

Fig. 8. TOC removal curves of 50% Ag/AgCl/Ag₂O photocatalyst under visible light.

ticles. Currently, the photogenerated electrons of Ag₂O transfer to the Ag nanoparticles to recombine with the plasmon-induced holes produced by plasmonic absorption of Ag nanoparticlesdue to its high Schottky barrier at the metal semiconductor interface, while the VB holes remain on Ag₂O to oxidize organic substances.
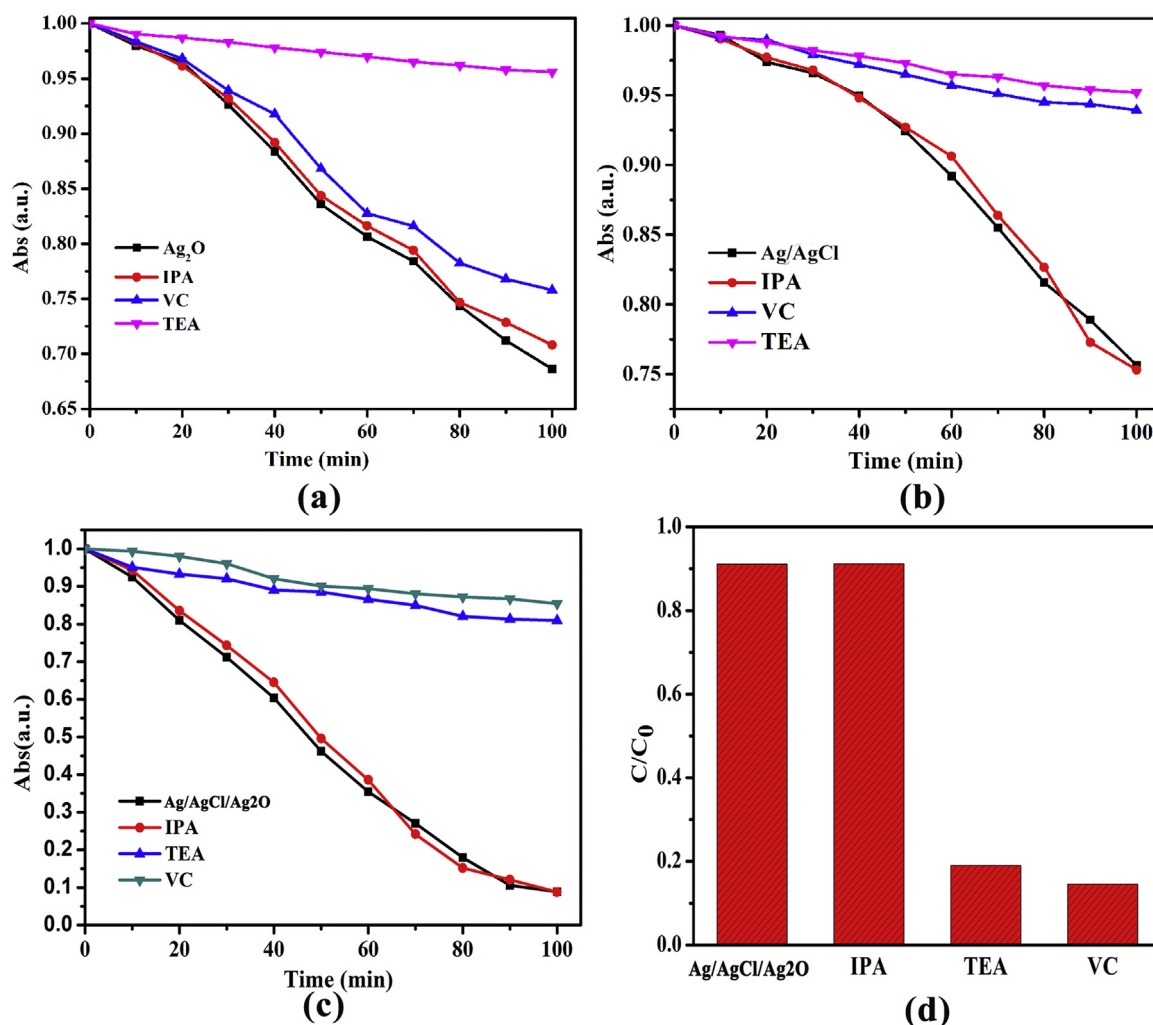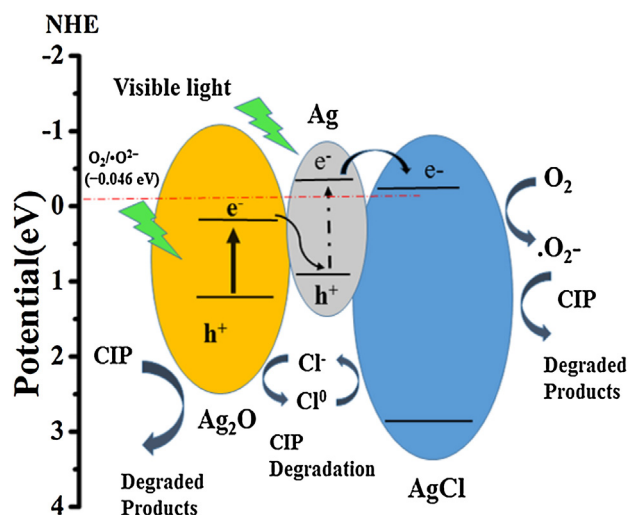
Fig. 9. The species trapping experiments for degradation of CIP over (a) pure Ag_2O, (b) AgCl and (c, d) 50% $Ag/AgCl/Ag_2O$.

Scheme 2. Proposed Photocatalytic Mechanism over the $Ag/AgCl/Ag_2O$ heterostructures.

Thus, such electrontransfer from Ag to a semiconductor should be expected to facilitate the photoexcited electron to be separated from recombination with the hole. In addition, due to the existence of Cl^- ions in the reaction solution, holes can transfer to the AgCl

surface corresponds to the oxidation of Cl^- ions to Cl^0 atoms. As chlorine atoms are reactive radical species, they should be able to oxidize CIP and hence become reduced to chloride ions again [42]. Moreover, the assemblage of Ag/AgCl nanocrystals on the surfaces of the Ag_2O formed a hierarchical nanostructure, which provided a high surface area and a large number of interfaces between the Ag/AgCl and Ag_2O samples. The high surface areas and large number of interfaces accessible to the outer environment could provide more active sites for the photocatalytic degradation of CIP molecules [23]. For these reasons, the $Ag/AgCl/Ag_2O$ heterostructures exhibit excellent photocatalytic performance.

4. Conlusions

In summary, we firstly designed a new system a plasmonic Z-scheme $Ag/AgCl/Ag_2O$ heterostructures via a facile in-suit growth strategy. The photocatalytic activities were evaluated by the degradation of Ciprofloxacin (CIP) under visible light irradiation ($\lambda > 420$ nm). The optimum photocatalytic efficiency of 50% $Ag/AgCl/Ag_2O$ heterostructures for the degradation of ciprofloxacin under visible light irradiation ($\lambda > 420$ nm) was about 2.9 and 3.73 times higher than that of individual Ag_2O and Ag/AgCl, respectively. The improved photocatalytic activities were attributed to the positively synergistic effects of the Ag/AgCl and Ag_2O substrates in effective separation of photogenerated electrons and holes, and the hierarchical structures of heterostructure with more surface active

sites for the decomposition of organic substances. This work will be useful for the design of highly efficient and stable photocatalysts for application in energy conversion and environmental remediation.

Acknowledgments

References

[1] Y. Yan, S.F. Sun, Y. Song, X. Yan, W.S. Guan, X.L. Liu, W.D. Shi, J. Hazard. Mater. 250–251 (2013) 106–114.
[2] M. Bobu, A. Yediler, I. Siminiceanu, S. Schulte-Hostede, Appl. Catal. B: Environ. 83 (2008) 15–23.
[3] M. Sturini, A. Speltini, F. Maraschi, A. Profumo, L. Pretali, E.A. Irastorza, E. Fasani, A. Albini, Appl. Catal. B: Environ. 119–120 (2012) 32–39.
[4] X.V. Doorslaer, K. Demeestere, P.M. Heynderickx, H.V. Langenhove, J. Dewulf, Appl. Catal. B: Environ. 101 (2011) 540–547.
[5] J.A.L. Perinia, M. Perez-Moyab, R.F. Nogueiraa, J. Photochem. Photobiol. A: Chem. 259 (2013) 53–58.
[6] J.J. Tu, Z.D. Yang, C. Hu, J.H. Qu, J. Environ. Sci. 26 (2014) 1154–1161.
[7] C.Y. Lu, W.S. Guan, T.K.A. Hoang, J.F. Guo, H.G. Gou, Y.L. Yao, J. Mater. Sci.: Mater. Electron. 27 (2016) 1966–1973.
[8] X.X. Zhang, R.P. Li, M.K. Jia, S.L. Wang, Y.P. Huang, C.C. Chen, Chem. Eng. J. 274 (2015) 290–297.
[9] T.A. Gad-Allah, M.E.M. Ali, M.I. Badawy, J. Hazard. Mater. 186 (2011) 751–755.
[10] A. Hassania, A. Khataeeb, S. Karacaa, J. Mol. Catal. A: Chem. 409 (2015) 149–161.
[11] M. El-Kemary, H. Shamy, I. Mehasseb, J. Lumin. 130 (2010) 2327–2331.
[12] M. Wu, J.M. Yan, X.W. Zhang, M. Zhao, Q. Jiang, J. Mater. Chem. A 3 (2015) 15710–15714.
[13] M.M. Rahman, S.B. Khan, A. Jamal, M. Faisal, A.M. Asiri, Chem. Eng. J. 192 (2012) 122–128.
[14] F.T. Chen, Z. Liu, Y. Liu, P.F. Fang, Y.Q. Dai, Chem. Eng. J. 221 (2013) 283–291.
[15] H.T. Ren, S.Y. Jia, Y. Wu, S.H. Wu, T.H. Zhang, X. Han, Ind. Eng. Chem. Res. 53 (2014) 17645–17653.
[16] C.L. Yu, G. Li, S. Kumar, K. Yang, R.C. Jin, Adv. Mater. 26 (2014) 892–898.
[17] Y.P. Bi, S.X. Ouyang, J.Y. Cao, J.H. Ye, Phys. Chem. Chem. Phys. 13 (2011) 10071–10075.
[18] P. Wang, B.B. Huang, X.Y. Qin, X.Y. Zhang, Y. Dai, J.Y. Wei, M.H. Whangbo, Angew. Chem. Int. Ed. 47 (2008) 7931–7933.
[19] L. Han, P. Wang, C.Z. Zhu, Y.M. Zhai, S.J. Dong, Nanoscale 3 (2011) 2931–2935.
[20] C.H. An, S. Peng, Y.G. Sun, Adv. Mater. 22 (2010) 2570–2574.
[21] H.B. Zhang, Y.G. Lu, H. Liu, J.Z. Fang, Nanoscale 7 (2015) 11591.
[22] M.S. Zhu, P.L. Chen, M.H. Liu, J. Mater. Chem. 22 (2012) 21487–21494.
[23] R. Qiao, M.M. Mao, E.L. Hu, Y.J. Zhong, J.Q. Ning, Y. Hu, Inorg. Chem. 54 (2015) 9033–9039.
[24] M.S. Zhu, P.L. Chen, M.H. Liu, ACS Nano 5 (2011) 4529–4536.
[25] Y.M. Wu, L. Li, Z. Li, A. Kinaci, K.Y. Chan, Y.G. Sun, J. R. ACS Nano 10 (2016) 3738–3746.
[26] H.Y. Li, Y.J. Sun, B. Cai, S.Y. Gan, D.X. Han, L. Niu, T.S. Wu, Appl. Catal. B: Environ. 170–171 (2015) 206–214.
[27] Y.H. Liang, S.L. Lin, L. Liu, J.S. Hu, W.Q. Cui, Appl. Catal. B: Environ. 164 (2015) 192–203.
[28] S.W. Zhang, J.X. Li, X.K. Wang, Y.S. Huang, M.Y. Zeng, J.Z. Xu, ACS Appl. Mater. Interfaces 6 (2014) 22116–22125.
[29] Y.X. Tang, V.P. Subramaniam, T.H. Lau, Y.K. Lai, D.G. Gong, P.D. Kanhere, Y.H. Cheng, Z. Chen, Z.L. Dong, Appl. Catal. B: Environ. 106 (2011) 577–585.
[30] D.L. Chen, T. Li, Q.Q. Chen, J.B. Gao, B.B. Fan, J. Li, X.J. Li, R. Zhang, J. Sun, L. Gao, Nanoscale 4 (2012) 5431.
[31] J.G. Hou, C. Yang, Z. Wang, Q.H. Ji, Y.T. Li, G.C. Huang, S.Q. Jiao, H.M. Zhu, Appl. Catal. B: Environ. 142–143 (2013) 579–589.
[32] L.Q. Ye, J.Y. Liu, C.Q. Gong, L.H. Tian, T.Y. Peng, L. Zan, ACS Catal. 2 (2012) 1677–1683.
[33] W.J. Zhou, H. Liu, J.Y. Wang, D. Liu, G.J. Du, J.J. Cui, ACS Appl. Mater. Interfaces 2 (2010) 2385–2392.
[34] X. Chen, Z. Guo, W.H. Xu, H.B. Yao, M.Q. Li, X.J. Huang, S.H. Yu, Adv. Funct. Mater. 21 (2011) 2049–2056.
[35] D.B. Xu, W.D. Shi, C.J. Song, M. Chen, S.B. Yang, W.Q. Fan, B.Y. Chen, Appl. Catal. B: Environ. 191 (2016) 228–234.
[36] P. Wang, B. Huang, Z. Lou, X. Zhang, X. Qin, Y. Dai, Z. Zheng, X. Wang, Chem.; Eur. J 16 (2010) 538–544.
[37] S.F. Kang, Y. Fang, Y.K. Huang, L.F. Cui, Y.Z. Wang, H.F. Qin, Y.M. Zhang, X. Lia, Y.G. Wang, Appl. Catal. B: Environ. 168–169 (2015) 472–482.
[38] S. Kumar, A. Baruah, S. Tonda, B. Kumar, V. Shanker, B. Sreedhar, Nanoscale 6 (2014) 4830.
[39] J.X. Xia, Y.P. Ge, D.X. Zhao, J. Di, M.X. Ji, S. Yin, H.M. Li, R. Chen, CrystEngComm 17 (2015) 3645.
[40] V. Maeda, ACS Catal. 3 (2013) 1486–1503.
[41] J. Tian, R. Liu, G.H. Wang, Y. Xu, X.F. Wang, H.G. Yu, Appl. Surf. Sci. 319 (2014) 324–331.
[42] Y. Wang, L.X. Liu, L. Xu, X.X. Cao, X.H. Li, Y.J. Huang, C.M. Meng, Z.G. Wang, W.J. Zhu, Nanoscale 69 (2014) 6790.